Horizon 2020
European Union funding
for Research & Innovation

ITS 4 LAND
innovations for land tenure

Deliverable 5.1
Technical Report

31 January 2018

Version 1.0

Abstract:
Technical report and software prototype on methods to automatically map features in orthoimages

Project Number: 687828
Work Package: 5
Lead: UT
Type: DEM
Dissemination: PU
Delivery Date: 31 January 2018
Contributors: Sophie Crommelinck, Mila Koeva, Michael Ying Yang, George Vosselman, Serene Ho, Ine Buntinx, Joep Crompvoets, Kaspar Kundert, Jan Sahib, Gordon Wayumba

Its 4 Land
Hengelosestraat 99
Enschede 7500AE
Netherlands
Phone: +31534874532
www.its4land.com

The its4land consortium consists of the following partners:

University of Twente (UT)
KU Leuven (KUL)
Westfaelische Wilhelms-Universitaet Muenster (WWU)
Hansa Luftbild AG (HL)
Institut d'Enseignement Superieur de Ruhengeri (INES)
Bahir Dar University (BDU)
Technical University of Kenya (TUK)
ESRI Rwanda (ESRI).

Its 4 Land
Hengelosestraat 99
Enschede 7500AE
Netherlands
Phone: +31534874532
www.its4land.com

Executive Summary

Unmanned aerial vehicles (UAV) are evolving as an alternative tool to acquire land tenure data. UAVs can capture geospatial data at high quality and resolution in a cost-effective, transparent and flexible manner, from which visible land parcel boundaries, i.e., cadastral boundaries are delineable. This delineation is not fully automated, even though physical objects automatically retrievable through image analysis methods mark a large portion of cadastral boundaries.

WP5 contributes to advancements in developing a corresponding methodology for UAV-based delineation of visible cadastral boundaries. It is designed for areas, in which object contours are clearly visible and coincide with cadastral boundaries. The methodology partly automates and facilitates the delineation of visible cadastral boundaries as follows: it combines image analysis methods, namely Globalized Probability of Boundaries (gPb) contour detection and Simple Linear Iterative Clustering (SLIC) superpixels. The approach chosen is realized based on a Random Forest (RF) classification combining feature information into a cost value per SLIC line, i.e., assigning low cost values to road outlines. The user-selected nodes are then connected along the least-cost path of weighted SLIC lines. The interactive part allows the user to edit and finalize the lines. It is implemented as a publically available QGIS plugin.

This report focusses on technical aspects of the described methodology and provides details on methods and implementations.

Contents

Abbreviations

DSM	Digital Surface Model
DTM	Digital Terrain Model
GCP	Ground Control Points
GIS	Geographical Information System
GNSS	Global Navigation Satellite System
gPb	Globalized Probability of Boundaries
GSD	Ground Sample Distance
GUI	Graphical User Interface
RF	Random Forest
RGB	Red Green Blue
SLIC	Simple Linear Iterative Clustering
UAV	Unmanned Aerial Vehicle

1. Introduction

its4land is a European Commission Horizon 2020 project funded under its Industrial Leadership program, specifically the 'Leadership in enabling and industrial technologies – Information and Communication Technologies ICT (H2020-EU.2.1.1.)', under the call H2020-ICT-2015 – and the specific topic – 'International partnership building in low and middle income countries' ICT-39-2015.

Its4land aims to deliver an innovative suite of land tenure recording tools that respond to sub Saharan Africa's immense challenge to rapidly and cheaply map millions of unrecognized land rights in the region. ICT innovation is intended to play a key role. Many existing ICT-based approaches to land tenure recording in the region have failed: disputes abound, investment is impeded, and the community's poorest lose out. its4land seeks to reinforce strategic collaboration between the EU and East Africa via a scalable and transferrable ICT solution. Established local, national, and international partnerships seek to drive the project results beyond R&D into the commercial realm. its4land combines an innovation process with emerging geospatial technologies, including smart sketchmaps, UAVs, automated feature extraction, and geocloud services, to deliver land recording services that are end-user responsive, market driven, and fit-for-purpose. The transdisciplinary work also develops supportive models for governance, capacity development, and business capitalization. Gender sensitive analysis and design is also incorporated. Set in the East African development hotbeds of Rwanda, Kenya, and Ethiopia, its4land falls within TRL 5-7: 3 major phases host 8 work packages that enable contextualization, design, and eventual land sector transformation. In line with Living Labs thinking, localized pilots and demonstrations are embedded in the design process. The experienced consortium is multi-sectorial, multi-national, and multidisciplinary. It includes SMEs and researchers from 3 EU countries and 3 East African countries: the necessary complementary skills and expertise is delivered. Responses to the range of barriers are prepared: strong networks across East Africa are key in mitigation. The tailored project management plan ensures clear milestones and deliverables, and supports result dissemination and exploitation: specific work packages and roles focus on the latter.

1.1. Application of Unmanned Aerial Vehicles

Unmanned Aerial Vehicles (UAVs) have emerged as rapid, efficient, low-cost and flexible acquisition systems for remote sensing data [1]. The data acquired can be of high-resolution and accuracy, ranging from a sub-meter level to a few centimes [2,3]. A photogrammetric UAV workflow includes flight planning, image acquisition, image orientation and data processing. The results include Digital Terrain Models (DTMs), Digital Surface Models (DSMs), orthoimages and point clouds [4]. UAVs are described as capable sourcing tools for remote sensing data, since they allow flexible maneuvers, capture of high-resolution imagery, flights under clouds, easy launch and landing and fast data acquisition at low cost. Disadvantages include payload limitations, uncertain or restricting airspace regulations, battery induced short flight duration, and time consuming processing of large volumes of data gathered [5,6]. In addition, multiple factors that influence the accuracy of derived products require extensive consideration. They include the quality of the camera, the camera calibration, the number and location of ground control points and the choice of processing software [7]. UAVs have been employed in a variety of applications such as the documentation of archaeological sites and cultural heritage [8,9], vegetation monitoring in favor of precision agriculture [10,11], traffic monitoring [12], disaster management [13,14] and 3D reconstruction [15].

Another emerging application field for UAV-based surveys is cadastral mapping. Cadastral maps are spatial representations of cadastre surveys, showing the extent, value and ownership of land [16]. Cadastral maps are intended to provide a positional description and identification of land parcels, which are crucial for a continuous and sustainable recording of land rights [17]. Furthermore, cadastral maps support land and property taxation, allow the development and monitoring of a land markets, support urban planning and infrastructure development and allow the production of statistical data. An extensive review on concepts and purposes of cadasters in relation to land administration is provided in [18,19]. UAVs are proposed as a new tool for fast and cheap spatial data acquisition and production enabling the production of cadastral maps. UAVs facilitate land administration processes and contribute to securing land tenure rights and provide a new approach to the establishment and updating of cadastral maps [20]. This contributes to new concepts in land administrations such as fit-for-purpose [21], pro-poor [22] and responsible land administration [23].

1.2. Application of UAV-based Cadastral Mapping

In the context of contemporary cadastral mapping, UAVs are increasingly emerging as tools to generate accurate and georeferenced high-resolution imagery. From these image data, cadastral boundaries can be visually detected and digitized [24-26]. In order to support digitization, existing parcel boundaries can be automatically superimposed, which could facilitate and accelerate cadastral mapping [27]. With the exception of [1,28], cadastral mapping is not mentioned in review papers as one of the application fields of UAVs [29-31]. This might be due to the small number of case studies in this field, the often highly prescribed legal regulations relating to cadastral surveys, and the novelty of UAV in mapping generally. Nevertheless, all existing case studies underline the high potential of UAVs for cadastral mapping – in both urban and rural contexts for developing and developed countries.

In developing countries, cadastral mapping contributes to the creation of formal systems for registering and safeguarding land rights. According to the World Bank and the International Federation of Surveyors (FIG), 75% of the world's population do not have access to such systems. Further, they state that 90 countries lack land registration systems, while 50 countries are in the process of establishing such systems [21]. In these countries, cadastral mapping is often based on ground survey methods or on partly outdated or unrectified aerial or satellite imagery of low-resolution, which can include areas covered by clouds. Numerous studies have investigated cadastral mapping based on orthoimages derived from satellite imagery [23,32-38] or aerial photography [39]. The definition of boundary lines is often conducted in a collaborative process among members of the communities, governments and aid organizations, which is referred to as 'Community Mapping' [40], 'Participatory Mapping' [23] or 'Participatory GIS' [32]. Outdated satellite imagery of low-resolution can be substituted for up-to-date high-resolution orthoimages derived from UAVs as is shown in case studies in

Namibia [25] and Rwanda [24]. The latter case shows the utility of UAVs to partially update existing cadastral maps.

In developed countries, the case studies focus on the conformity of the UAV data's accuracy with local accuracy standards and requirements [41,42]. Furthermore, the case studies tend to investigate possibilities of applying UAVs to reshape the cadastral production line efficiency and effectiveness [7,43,44]. When applying UAVs, manual boundary detection with all stakeholders is conducted in an office, eliminating the need for convening all stakeholders on the parcel. In developed countries, UAV data are frequently used to update small portions of existing cadastral maps rather than creating new ones. Airspace regulations are the most limiting factor that hinder the thorough use of UAVs. Currently, regulatory bodies face the alignment of economic, information and safety needs or demands connected to UAVs [31,45]. Once these limitations are better aligned with societal needs, UAVs might be employed for land administration, as well as for further purposes such as the monitoring of public infrastructure like oil and gas pipelines, power lines, dikes, highways, and railways [46]. Nowadays, some national mapping agencies in Europe integrate, but mainly investigate, the use of UAVs for cadastral mapping [45].

Overall, UAVs can be employed to support land administration both in creating and updating cadastral maps. The entirety of case studies confirms that UAVs are suitable as an addition to conventional data acquisition methods in order to create detailed cadastral maps including overview images or 3D models [41,42,47]. The average geometrical precision is shown to be the same, or better, compared to conventional terrestrial surveying methods [7]. UAVs will not substitute conventional approaches, since they are currently not suited to map large areas such as entire countries [48]. The use of UAVs supports the economic feasibility of land administration and contributes to the accuracy and completeness of cadastral maps.

1.3. Boundary Delineation for UAV-based Cadastral Mapping

In published case studies, cadastral boundaries are manually detected and digitized from orthoimages. This is realized either in an office with a small group of stakeholders – for one parcel or in a community mapping approach for several parcels at once. None of the case studies applies an automatic approach to extract boundary features from the UAV data. An automatic or semi-automatic feature extraction process would facilitate cadastral mapping: manual feature extraction is generally regarded as time-consuming, wherefore an automation will bring substantial benefits [4].

Jazayeri et al. (2014) state that UAV data are an accurate and low-cost approach for automated object reconstruction and boundary extraction. This is especially true for visible boundaries, physically manifested by objects such as hedges, stone walls, large scale monuments, walkways, ditches or fences, which often coincide with cadastral boundaries [50,51]. Such visible boundaries bear the potential to be automatically extracted from UAV data. However, to the best of the authors' knowledge, no research has been done on expediting cadastral mapping through automatic boundary delineation from UAV data.

1.4. Cadastral Boundary Characteristics

Different approaches exist to categorize concepts of cadastral boundaries. The lines between the different categories visualized in Figure 1 can be understood as fuzzy. From a technical point of view, cadastral boundaries can be divided into two categories: (i) fixed boundaries, whose accurate spatial position has been recorded and agreed upon and (ii) general boundaries, whose precise spatial position is left undetermined [52]. Both require surveying and documentation in cadastral mapping.

Cadastral surveying consists of (i) direct techniques, in which the accurate spatial position of a boundary is measured and fixed on the ground using theodolite, total stations and Global Navigation Satellite System (GNSS); and (ii) indirect techniques, in which remotely sensed data such as aerial or satellite imagery are applied with minimal ground verification. The spatial position of boundaries is derived from these data in a second step [33]. Fixed boundaries are commonly measured with direct techniques, which provide the required higher accuracy. Indirect techniques, including UAVs, are able to determine fixed boundaries only in the case of high-resolution data. Indirect techniques are mostly applied to extract visible boundaries through image interpretation and boundary tracing. These boundaries are represented by physical objects, which coincide with the concept of general boundaries [50,51].

In Kenya for example, the general boundaries were originally derived from ground survey methods of chain, campus and plane table. These boundaries were instantly drawn onto a sheet of paper attached to the plane table. This method was later found to be too slow for the vast area to be covered and the government reverted to the use of aerial photos. Initially, these photos were ortho-rectified to take care of tilt and relief distortions. These surveys were carried out in the Central Region of Kenya at the time of the Mau Mau wars in order to check the quality of the Plane Table surveys.

The ortho-rectifications were carried out in London as the technology was not yet available in Kenya. This process was later abandoned as it was too slow and expensive for the African peasants who were eagerly waiting for first registration. The government thereafter used simple tracings from the photos to produce temporary and interim maps called the Preliminary Index Diagrams (PIDs) for the first registration [53]. These PIDs are still being used for registration of land adjudicated areas to the present day.

This report concentrates on methods delineating general, i.e., visible cadastral boundaries from high-resolution data applying indirect surveying techniques. The methods are intended to automatically extract boundary features from UAV data.

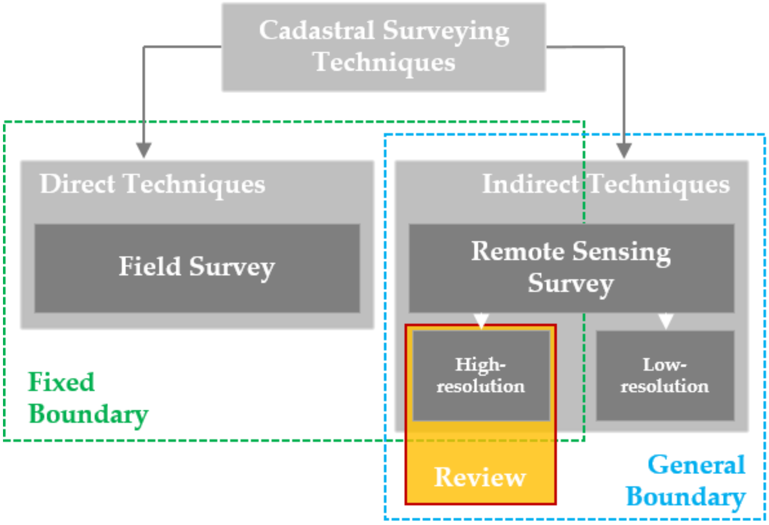

Figure 1. Overview of cadastral surveying techniques and cadastral boundary concepts that contextualize the scope of this research. The lines between different categories are fuzzy and should not be understood exclusively. They are drawn to give a general overview.

In order to understand, which visible boundaries define the extents of land and to identify common boundary characteristics, literature on 2D cadastral mapping – based on indirect techniques – was reviewed. Man-made objects are found to define cadastral boundaries as well as natural objects. Studies name buildings, hedges, fences, walls, roads, footpaths, pavement, open areas, crop type, shrubs, rivers, canals and water drainages as cadastral boundary features [7,25,32,33,35,54-56]. Trees are named as the most limiting factor since they often obscure the view of the actual boundary [42,57].

No study summarizes characteristics of detected cadastral boundaries, even though it is described as crucial for feature recognition to establish a model describing the general characteristics of the feature of interest [58]. Common in many approaches is the linearity of extracted features. This may be due to the fact that some countries do not accept curved cadastral boundaries [34]. Even if a curved river marks the cadastral boundary, the boundary line is approximated by a polygon [33].

When considering named features, the following characteristics can be observed: most features have a continuous and regular geometry expressed in long straight lines of a limited curvature. Furthermore, features often share common spectral properties, such as similar values in color and texture. Moreover, boundary features are topologically connected and form a network of lines that surround land parcels of a certain (minimal) size and shape. Finally, boundaries can be indicated by a special distribution of other objects such as trees. In summary, general boundary features are detectable based on their geometry, spectral property, topology, and context.

This report focusses on methods that extract linear boundary features, since cadastral boundaries are commonly represented by straight lines with exceptions outlined in [59,60]. Cadastral representations in 3D as described in [61] are excluded.

UAVs cannot detect all cadastral boundaries. Only visible boundaries that are detectable with an optical sensor can be extracted using UAVs. This approach does not consider socially perceived boundaries not marked by a physical object.

Figure 2 provides an overview of visible boundary characteristics mentioned above and commonly raised issues in terms of their detection. The cadastral boundaries are derived based on (a) roads, power lines and pipelines [48]; (b) fences and hedges [25]; (c), (d) crop types [42]; (f) roads, foot paths, water drainage, open areas and scrubs [62] and (e) adjacent vegetation [57]. Figure 2 (d) shows the case of a nonlinear irregular boundary shape. The cadastral boundaries in (e) and (f) are often obscured by tree canopy. Cadastral boundaries in (a), (b), (c) and (d) are derived from UAV data; in (e) and (f) from HRSI. All of the boundaries are manually extracted and digitized.

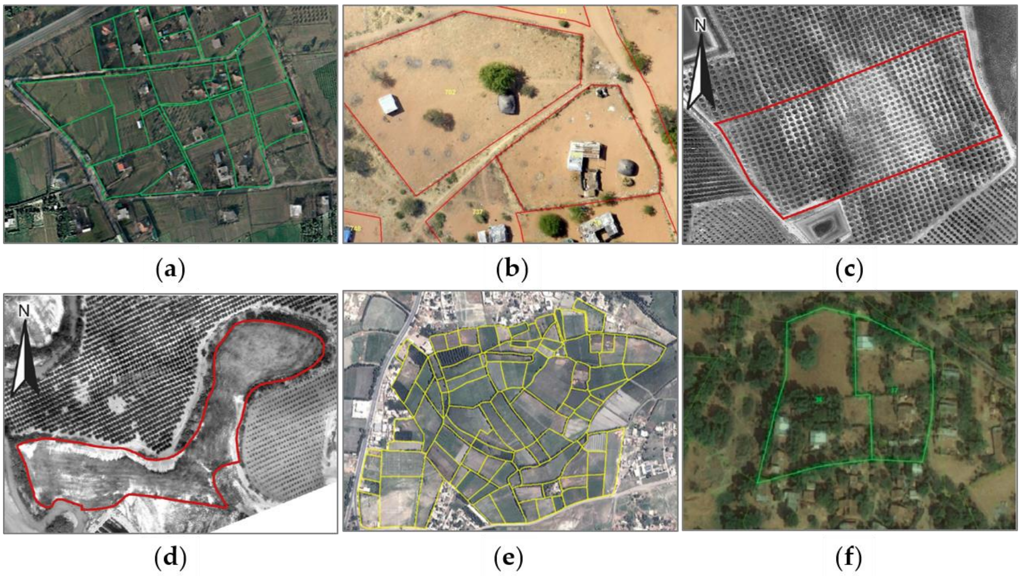

Figure 2. Characteristics of cadastral boundaries extracted from high-resolution optical remote sensors.

1.5. Boundary Delineation Workflow

In past work, a hypothetical generalized workflow for the automatic extraction of visible cadastral boundaries has been proposed [63]. It was derived from 89 studies that extract physical objects related to those manifesting cadastral boundaries from high-resolution optical sensor data. The synthesized methodology consists of image segmentation, line extraction and contour generation (Figure 3).

For image segmentation, globalized probability of boundary (gPb) contour detection was found to be applicable for an initial detection of visible boundaries. However, this method does not enable the processing of large images. Therefore, the UAV data were reduced in resolution, which consequently led to a reduced localization quality [64]. The localization quality at the locations of initially detected candidate boundaries is improved through the following: for line extraction, simple linear iterative clustering (SLIC) superpixels were found to coincide largely with object boundaries in terms of completeness and correctness [65]. For contour generation gPb contour detection and SLIC superpixels are combined with machine learning and processed in a semi-automatic procedure that allows a subsequent delineation of visible boundaries. This report describes each of these workflow steps in detail.

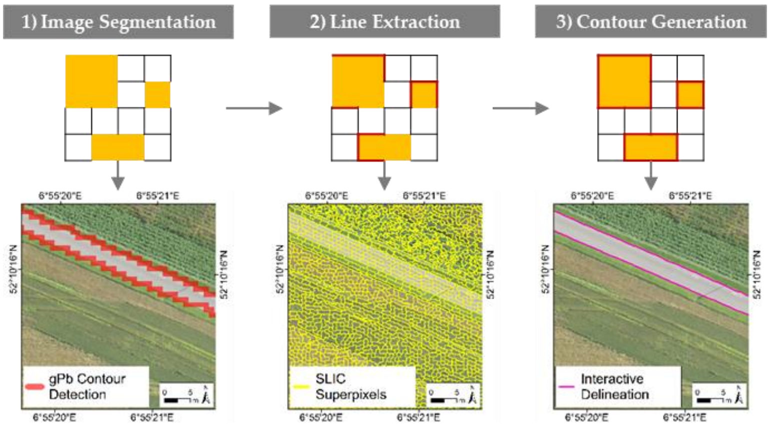

Figure 3. Sequence of a commonly applied workflow proposed in [63]. The workflow aims to extract physical objects related to those manifesting cadastral boundaries from high-resolution optical sensor data.

1.6. Report Objective and Structure

The literature review shows that automating UAV-based cadastral mapping is little investigated and bears potential to make cadastral mapping more reproducible, transparent, automated, scalable and cost-effective. Addressing this research gap is the aim of WP5 in the its4land project. This is done by designing and implementing a methodology for an automated delineation of visible cadastral boundaries from UAV data. This report describes the current functioning of such a methodology and provides implementation details.

The report is structured according to the main workflow steps visualized in Figure 4. Its implementation is summarized in Table 1 and available in [66]. Each of its main steps, i.e., data pre-processing, machine learning, and interactive outlining, is one section in the report. Each section, i.e., each workflow step, is divided into a description of its background and its practical realization with regards to the methodology development. The background part describes motivation and methods of each workflow step and provides references to these. The practical part describes implementation details of each workflow step and its manual or automatic functioning. In the case of a manual workflow step, all required steps are visualized with screenshots. In the case of an automatic workflow step, its functioning and implementation details, as well as input and output data, are visualized in a schematic figure.

The term methodology developed refers to the entire workflow. Workflow steps refer to each of the workflow components. Plugin refers to the implementation of the final workflow step, i.e., interactive outlining. The remaining workflow steps are implemented in script to be run in Python, Matlab, QGIS or GRASS GIS (Table 1).

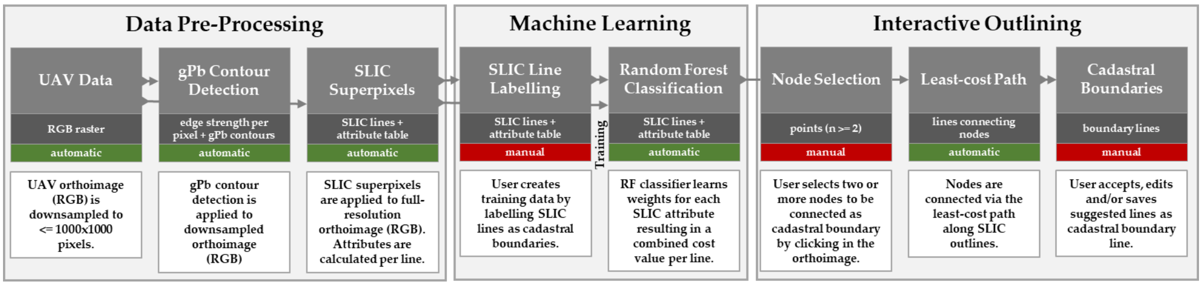

Figure 4. Delineation workflow.

Table 1. Implementation of delineating workflow.

Workflow step	Script	Software
Data pre-processing	A1_resizing	PyQGIS
	A2_gPb_contour_detection	Matlab
	A3_raster_to_centerline	PyQGIS
	A4_SLIC_superpixels	GRASS GIS
	A5_SLIC_raster_to_lines	PyQGIS
	A6_SLIC_attributes	PyQGIS
Machine learning	B1_RF_classification	Python
Interactive outlining	BoundaryDelineation (QGIS plugin)	PyQGIS

2. Data Pre-Processing

2.1. UAV Data

The following example implementation of the workflow is based on data from Amtsvenn, Germany (latitude/longitude: 52.17335/6.92865) shown in Figure 5. The data were captured with indirect georeferencing, i.e., Ground Control Points (GCPs) were distributed in the field and measured with a Global Navigation Satellite System (GNSS). The orthoimage captures an extent of 1000 x 1000 m and has a Ground Sample Distance (GSD) of 0.05 m. It was captured with a fixed-wing UAV (model: GerMAP G180, camera: Ricoh GR) flying with a forward overlap of 80% and a sideward overlap of 65%. The orthoimages were generated with Pix4DMapper software.

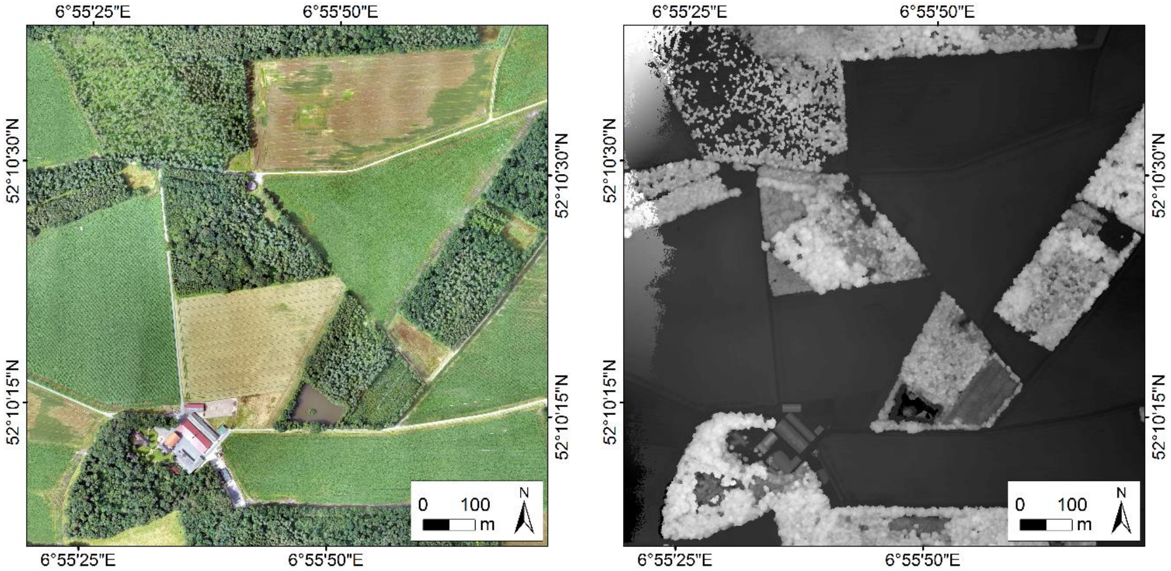

(a) **(b)**

Figure 5. UAV data of Amtsvenn, Germany showing an extent of 1000 x 1000 m with a GSD of 0.05 m as RGB (a) and DSM (b) orthoimages.

2.2. gPb Contour Detection

2.2.1. Background

Contour detection refers to detecting closed boundaries between objects or segments. Out of different approaches for an initial detection of candidate boundaries [63], the following method was found to work nearly optimal: globalized Probability of Boundary (gPb) contour detection. It refers to the processing pipeline visualized in Figure 6, explained in this section and based on [67]. This pipeline originating from computer vision aims to find closed boundaries between objects or segments in an image. This is achieved through combining edge detection and hierarchical image segmentation, while integrating image information on texture, color and brightness on both a local and a global scale.

In a first step, oriented gradient operators for brightness, color and texture are calculated on two halves of differently scaled discs. The cues are merged based on a logistic regression classifier resulting in a posterior probability of a boundary, i.e., an edge strength per pixel. The local image information is combined through learning techniques with global image information that is obtained through spectral clustering. The learning steps are trained on natural images from the 'Berkeley Segmentation Dataset and Benchmark' [68]. By considering image information on different scales, relevant boundaries are verified, while irrelevant ones, e.g., in textured regions, are eliminated. This is referred to as global optimization in the following.

In the second step, initial regions are formed from the oriented contour signal provided by a contour detector through oriented watershed transformation. Subsequently, a hierarchical segmentation is performed through weighting each boundary and their agglomerative clustering to create an ultrametric contour map that defines the hierarchical segmentation.

The overall result consists of (i) a contour map, in which each pixel is assigned a probability of being a boundary pixel, and (ii) a binary boundary map containing closed contours, in which each pixel is labeled as 'boundary' or 'no boundary' (Figure 9). The approach has been shown to be applicable to UAV orthoimages for an initial localization of candidate object boundaries [64]. UAV orthoimages of extents larger than 1000 x 1000 pixels need to be reduced in resolution, due to the global optimization of the original implementation. The localization quality of initially detected candidate boundaries is improved through the following workflow steps.

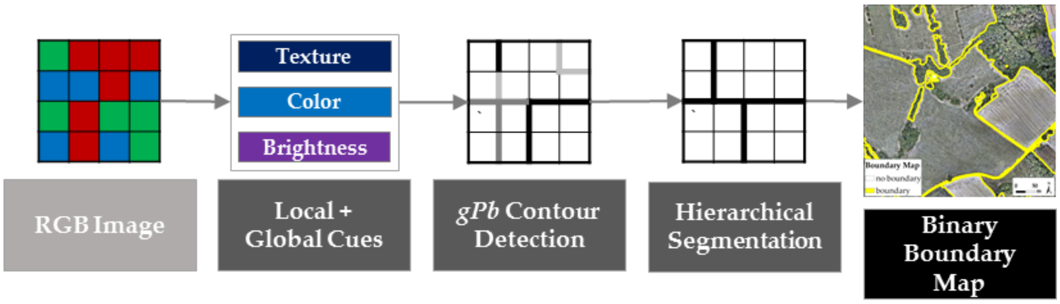

Figure 6. Processing pipeline of globalized probability of boundary (gPb) contour detection and hierarchical image segmentation resulting in a binary boundary map containing closed boundaries.

2.2.2. Realization

Due to the global optimization of the gPb contour detection approach, preventing the use of images with extents larger than 1000 x 1000 pixels, the RGB orthoimage is downsampled to <=1000 x 1000 pixels. This is done with a PyQGIS script (Figure 7).

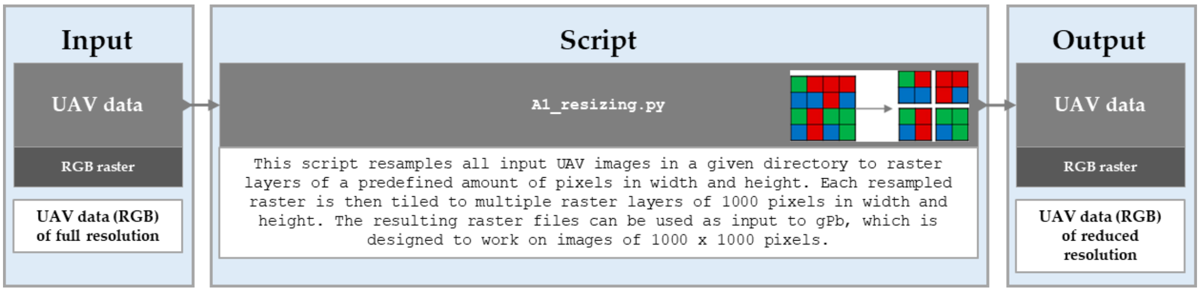

Figure 7. Schematic representation of downsampling script available in [66].

gPb contour detection is implemented in Matlab (Figure 8) [69] [69] [68] [69]. The source code is publicly available in [70]. The script requires a list of precompiled *.mex files in a `lib` directory and runs on Linux. That `lib` directory contains a `geotiffwrapper.m` script, in which the variable `A.ProjectedCSTypeGeoKey` needs to be set to the EPSG code of the input image. This ensures that the output *.tif files have the same georeferencing as the input images. All files in the `lib` directory are precompiled *.mex files, which are called via the main script (`gPb_ucm_final.m`). The images to be processed (*.tif and their *.tfw files) need to be copied to the `data` directory. An example output of gPb contour detection is shown in Figure 9.

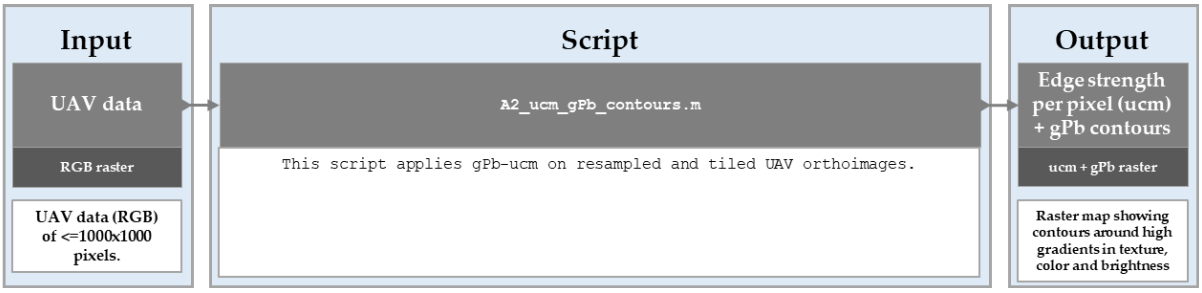

Figure 8. Schematic representation of gPb contour detection script available in [66].

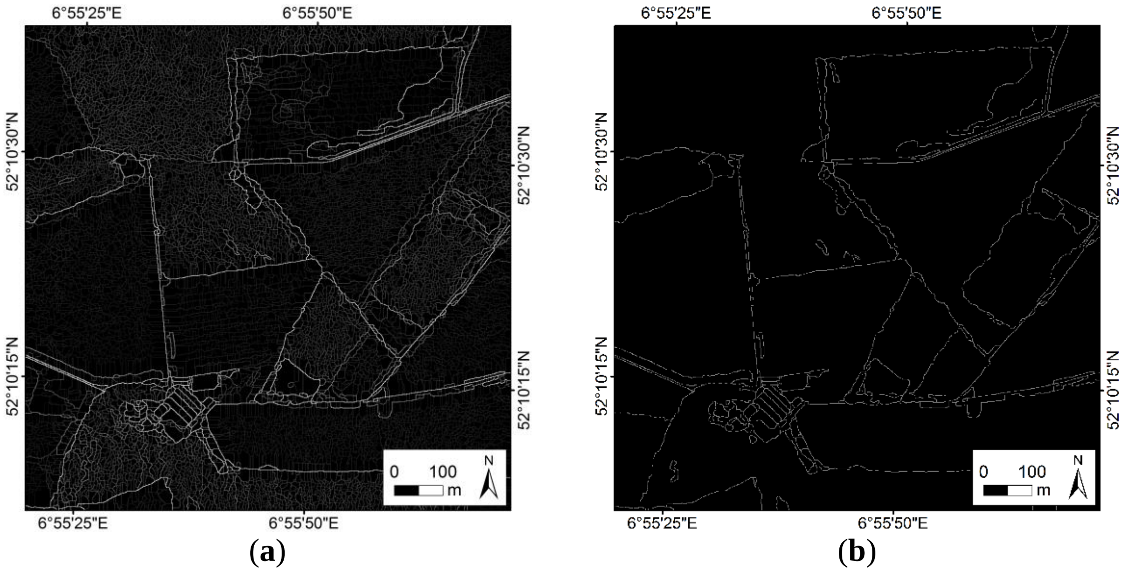

Figure 9. The result of gPb contour detection applied to the Amtsvenn UAV data (**Figure 2**). (**a**) shows a contour map, in which each pixel is assigned a probability of being a boundary pixel. (**b**) shows a binary boundary map containing closed contours, in which each pixel is labeled as 'boundary' or 'no boundary'.

The gPb raster map is transferred to a vector shapefile by keeping the centerline for each gPb contour. This is done with a PyQGIS script (Figure 10).

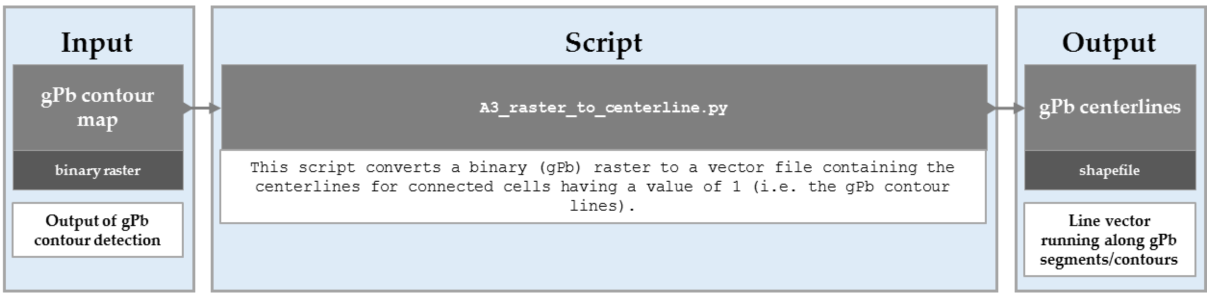

Figure 10. Schematic representation of raster to centerline conversion script available in [66].

2.3. SLIC Superpixels

2.3.1. Background

Simple linear iterative clustering (SLIC) superpixels originate from computer vision and are introduced in [71]. Superpixels aim to group pixels into perceptually meaningful atomic regions and can therefore be located between pixel- and object-based approaches. The approach allows to compute image features for each superpixel rather than each pixel, which reduces subsequent processing tasks in complexity and computing time. Further, the boundaries of superpixels adhere well to object outlines in the image and can therefore be used to delineate objects [72].

When comparing state-of-the-art superpixel approaches, SLIC superpixels have outperformed comparable approaches in terms of speed, memory efficiency, compactness and correctness of outlines [73-75]. The approach, visualized in Figure 11, was introduced and extended by Achanta el al. (2010, 2012). SLIC considers image pixels in a 5D space, in terms of their L*a*b values of the CIELAB color space and their x and y coordinates. Subsequently, the pixels are clustered based on an adapted k-means clustering. The clustering considers color similarity and spatial proximity. SLIC implementations are widely available. This study applies the GRASS implementation [78].

The approach has been shown to be applicable to UAV orthoimages of 0.05 m ground sample distance (GSD) [65]. Further, cadastral boundaries demarcated through physical objects often coincide with the outlines of SLIC superpixels.

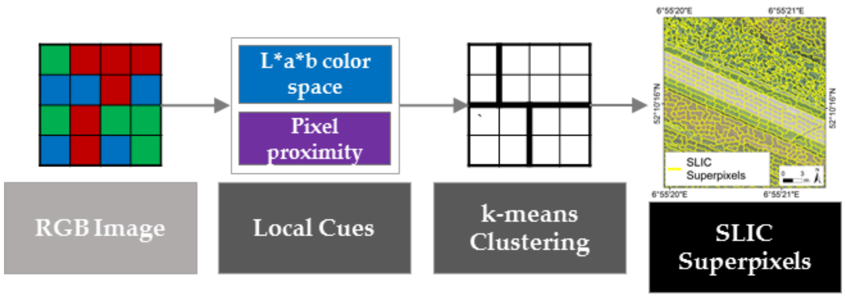

Figure 11. Processing pipeline of simple linear iterative clustering (SLIC) resulting in agglomerated groups of pixels, i.e., superpixels, whose boundaries outline physical objects in the image.

2.3.2. Realization

SLIC superpixels are created from the RGB orthoimage using a GRASS Add-on [79], which is executable in the GRASS GIS console [78]. The commands in `A4_SLIC_superpixels.txt` need to be entered in the GRASS console (Figure 12).

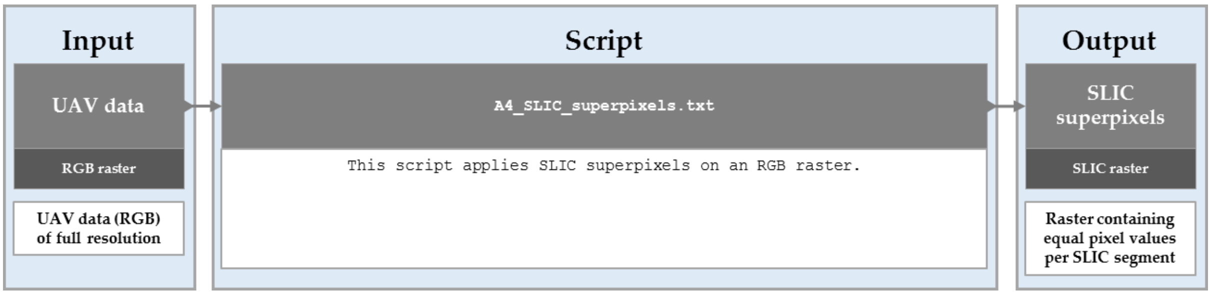

Figure 12. Schematic representation of SLIC superpixel script available in [66].

The SLIC raster map is transferred to a vector by keeping the outline of each SLIC segment as a vector polygon. The outline of each polygon is broken into several line segments, wherever two outlines of polygons intersect. This is done with a PyQGIS script (Figure 13).

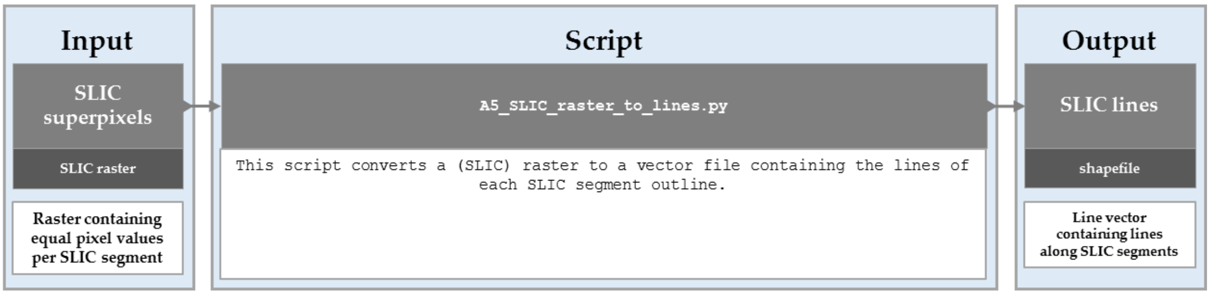

Figure 13. Schematic representation of raster to line conversion script available in [66].

For each SLIC line segment, different attributes are calculated by taking into account information from the gPb and ucm maps, the RGB and DSM orthoimages, as well as information on each line's geometry and topology (Table 2, Figure 14). All input layers are clipped to 3 m around the reference data to reduce processing time.

Table 2. Attributes calculated per SLIC line segment

Attribute	Description
length [m]	length per SLIC segment along the line
ucm_rgb	median of all ucm_rgb pixels underlying a SLIC segment
lap_dsm	median of all pixels from DSM laplacian filter underlying a SLIC segment
dist_to_gPb [m]	distance between SLIC segment and gPb lines (overall shortest distance)
azimuth [°]	horizontal angle measured clockwise from north per SLIC segment
sinuosity	ratio of distance between start and end point along SLIC segment (line length) and their direct Euclidean distance
azi_gPb [°]	horizontal angle measured clockwise from north per gPb segment closest to a SLIC segment (aims to indicate line parallelism/collinearity)
r_dsm_medi	median of all DSM values lying with a 0.2m buffer right of each SLIC segment
l_dsm_medi	median of all DSM values lying with a 0.2m buffer left of each SLIC segment
r_red_medi	median of all red values lying with a 0.2m buffer right of each SLIC segment
l_red_medi	median of all red values lying with a 0.2m buffer left of each SLIC segment
r_gre_medi	median of all green values lying with a 0.2m buffer right of each SLIC segment
l_gre_medi	median of all green values lying with a 0.2m buffer left of each SLIC segment
r_blue_med	median of all blue values lying with a 0.2m buffer right of each SLIC segment

l_blue_med	median of all blue values lying with a 0.2m buffer left of each SLIC segment
red_grad	absolute value of difference between r_red_medi and l_red_medi
green_grad	absolute value of difference between r_green_medi and l_green_medi
blue_grad	absolute value of difference between r_blue_medi and l_blue_medi
dsm_grad	absolute value of difference between r_dsm_medi and l_dsm_medi

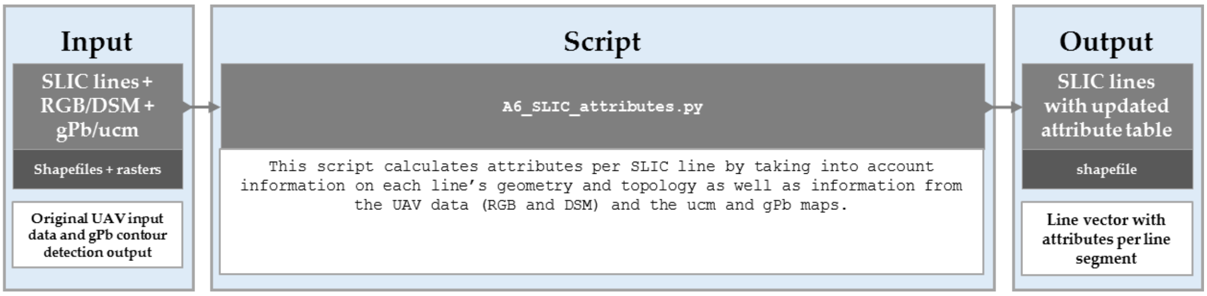

Figure 14. Schematic representation of attribute calculation script available in [66].

3. Machine Learning

3.1. SLIC Line Labelling

3.1.1. Background

The labelling of SLIC lines distinguishes between the two categories ‘boundary’ and ‘no boundary’. Each SLIC line segment that belongs to a visually detectable object that delineates a cadastral boundary should be labelled manually as ‘boundary’ by a human operator. This needs to be done for the training and validation data that are required for the subsequent classification.

3.1.2. Realization

The labelling can be done in any GIS software such as QGIS or ArcGIS. First, the SLIC line shapefile layer and the RGB layer are loaded. In the attribute table of the SLIC layer, all calculated attributes as well as one column named ‘boundary’ should be present. In the end, the ‘boundary’ column should be filled with ones (for ‘boundary’) and zeros (for ‘no boundary’). The following steps show, how this is realized in QGIS (Table 3).

Table 3. SLIC line labelling in QGIS

Step	Action	Screenshot
1	Load SLIC line shapefile layer and RGB layer in QGIS	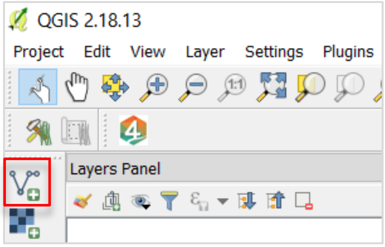
2	Select all line segments to be labelled as boundary (`Ctrl` + Left-Click to select multiple lines at once)	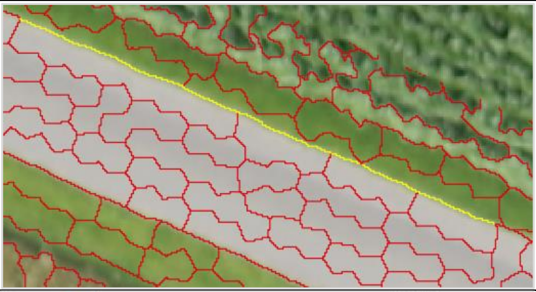
3	Open attribute table of SLIC line shapefile	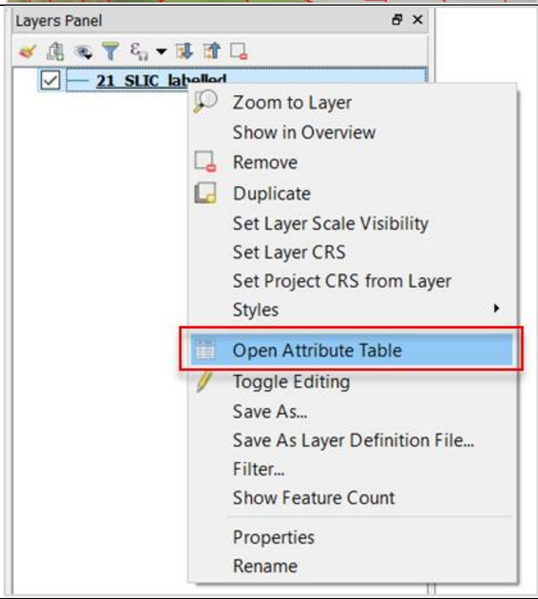
4	Start editing the layer	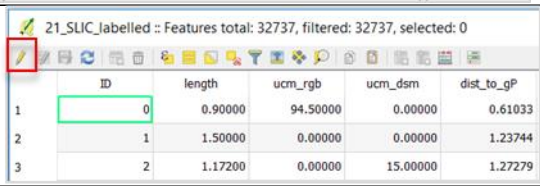
5	Change value for all selected features to boundary = 1, save edits and stop editing	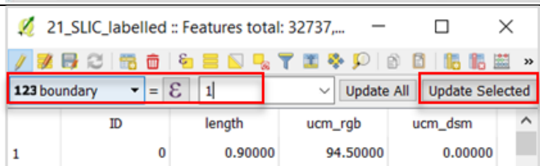

6	Save updated layer as *.csv file	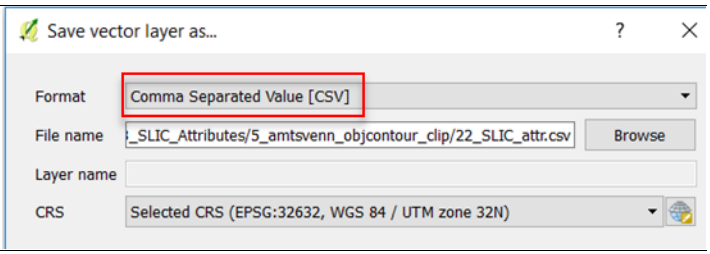

3.2. Random Forest (RF) Classification

3.2.1. Background

Contour generation aims to support the identification of a subset of superpixels, whose collective boundaries correspond to object contours in the image. This idea is based on work of Levinshtein et al., who first reformulated the problem of finding contour closure to finding subsets of superpixels aligned with object contours [80,81]. The authors combine features such as distance, strength, curvature and alignment to identify edges for image segmentation. These features are combined by learning the best generic weights for their combination on a computer vision benchmark dataset. This approach can be related to perceptual grouping in which local attributes in relation to each other are grouped to form a more informative attribute that contains context information [82]. By iteratively grouping low-level image descriptions, a higher-level structure of higher informative value is obtained [83]. Perceptual grouping for contour closure is widely applied in computer vision [84,85], pattern recognition [83] as well as in remote sensing to extract agricultural field boundaries [86] or roads [87]. The criteria for perceptual grouping are mostly based on the classical Gestalt cues of proximity, continuity, similarity, closure, symmetry, common regions and connectedness that originate from Lowe's early work on perceptual grouping, in which a computational model for parallelism, collinearity, and proximity is introduced [88]. The attributes are mostly combined into a cost function that models the perceptual saliency of the resulting structure.

The ideas described above are transferable to the workflow developed: Wegner et al. (2015) extract road networks from aerial imagery and elevation data by applying superpixel-based image segmentation, classifying the segments with a random forest (RF) classifier and searching for the Dijkstra least-cost path between segments with high probabilities of being roads. Warnke and Bulatov (2017) extend this approach by optimizing the methodology in terms of feature selection. They investigate the training step by evaluating two classifiers and show that choosing features largely influences classification quality and that feature importance depends on the selected classifier. Similarly, García-Pedrero et al. (2017) use superpixels as minimum processing units, which is followed by a classification-based agglomerating of superpixels to obtain a final segmentation of agricultural fields from satellite imagery. All these approaches consider superpixels as segments: superpixels are agglomerated by comparing features per segment in relation to its adjacent neighbors [90-92], sometimes in combination with boundary information [93,94].

To automate the delineation of cadastral boundaries, the problem of finding adjacent superpixels belonging to one object is reformulated to finding parts of superpixel outlines that delineate one object: attributes are not calculated per superpixel, but per outline (Figure 15). They are created by splitting each superpixel outline, wherever outlines of three or more adjacent superpixels have a point in common. Attributes per line are calculated to infer a weight indicating the likelihood of belonging to a (parcel) boundary line. Similar to the classical Gestalt cues, the attributes consider the SLIC lines themselves (i.e., their geometry) and their spatial context (i.e., their relation to gPb lines or to underlying RGB and DSM rasters). For training and validation, one attribute is added manually by labelling SLIC lines corresponding to reference object outlines as ‘boundary’ or ‘no boundary’, respectively. The data are divided into groups for training and validation. All attributes apart from the manual one are combined by a RF classifier producing a synthesized likelihood value per line in range [0; 1] for the validation data. This value is used to find the least-cost path between points indicated by a user. The points represent start-, end, and optionally middle-points of a boundary to be delineated. They are connected along SLIC lines via a Steiner least-cost path. Finally, the result is displayed to the user providing the options to accept, edit and/or save the line. This interactive outlining is implemented as an open source QGIS plugin [95].

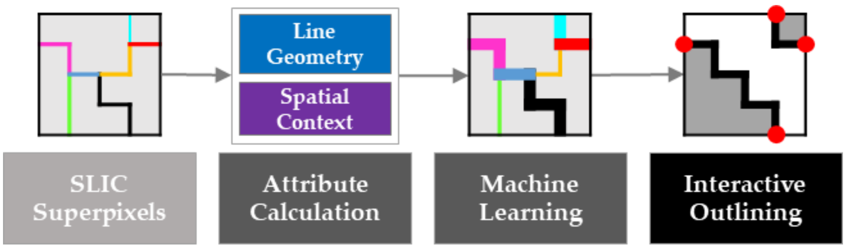

Figure 15. Processing pipeline of interactive delineation: each superpixel outline is split, wherever outlines of three or more adjacent superpixels have a point in common (visualized by line color). Attributes are calculated per line. They are combined with a RF classifier to produce likelihoods for being a boundary (visualized by line thickness). User-selected nodes (red points) are connected along lines of highest likelihoods.

3.2.2. Realization

The classification is implemented based on a scikit-learn Python implementation [96] of RF classification[97][97][96][97]. The script can be executed in a regular Python programming environment such as PyCharm (Figure 16).

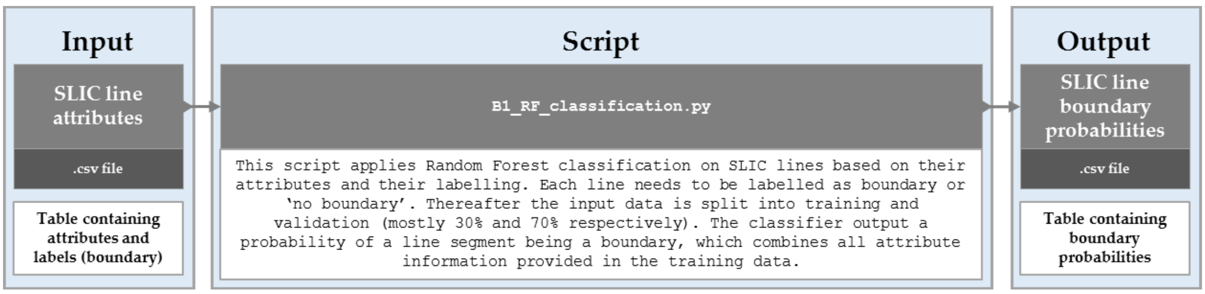

Figure 16. Schematic representation of RF classification script available in [66].

After classification, the *.csv file, i.e., the attribute table with the updated probabilities, needs to be merged to the shapefile of SLIC lines. Probabilities of lines being a boundary line are updated only for those belonging to the validation dataset. The referencing is done via the unique ID value (Table 4).

Table 4. Assigning RF probabilities to SLIC lines.

Step	Action	Screenshot
1	Load *.csv file as delimited text file	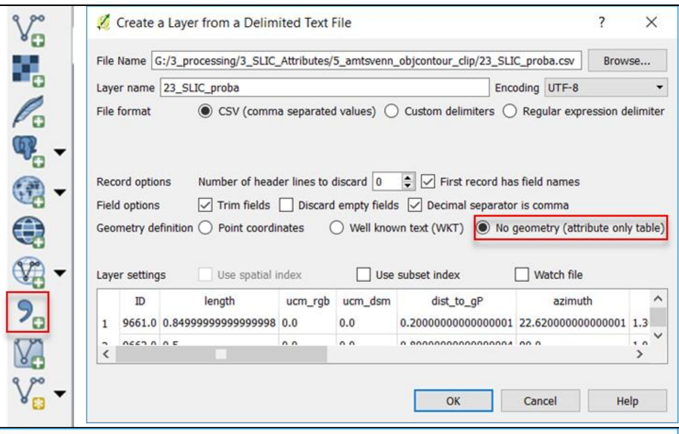
2	Change field type of ID to integer and save as ‘new_ID’	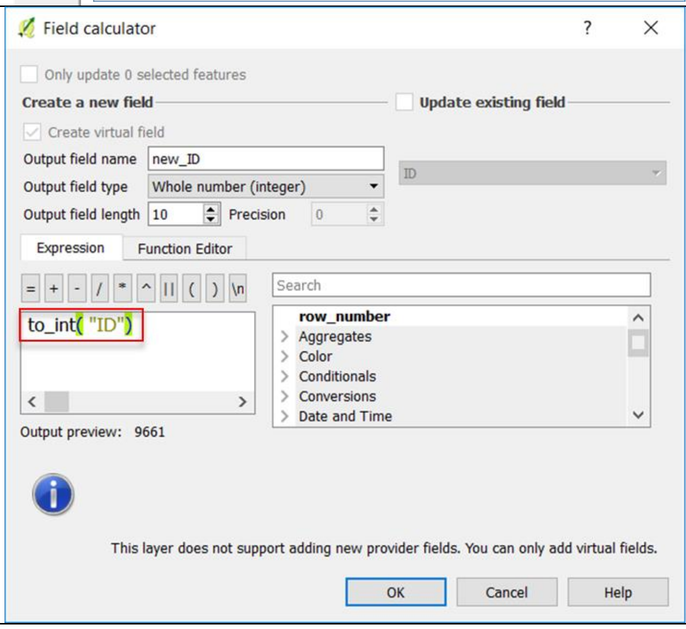

<table>
<tr>
<td>3</td>
<td>Join attribute tables of SLIC shapefile and refactored *.csv file based on ID value</td>
<td>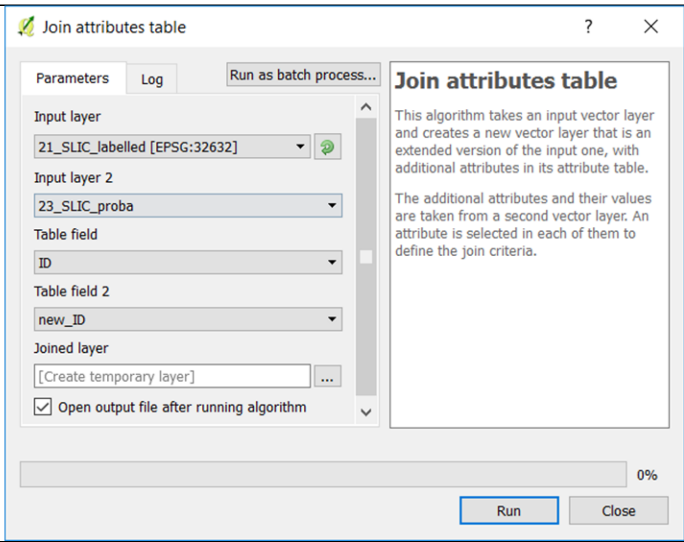
</td>
</tr>
<tr>
<td>4</td>
<td>Delete all fields in attribute table apart from ‘proba_bo’ with the ‘refactor field’ module (or in attribute table editor) and save as shapefile for further processing.

Make sure the field containing the probabilities per line segment has the name ‘proba_bo’.</td>
<td>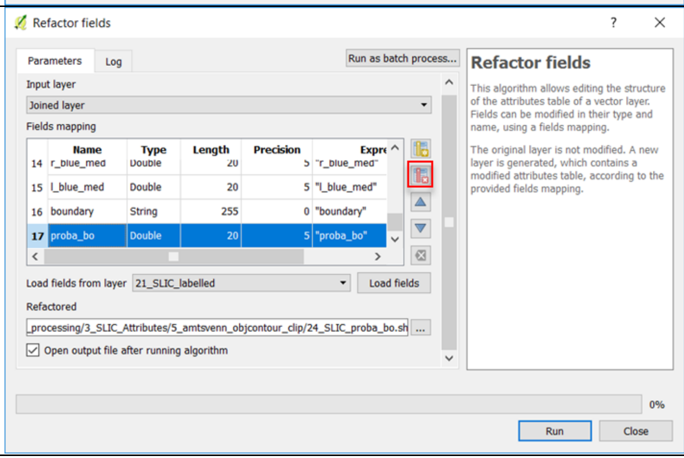
</td>
</tr>
</table>

4. Interactive QGIS Plugin

4.1. Plugin Workflow

4.1.1. Background

The QGIS plugin combines the detection quality of gPb contour detection with the localization quality of SLIC superpixels. Furthermore, it allows the user to interactively finalize detected contours to cadastral boundaries by connecting subsets of superpixels, whose collective boundaries correspond to object contours in the image. The plugin workflow consists of two parts: (i) First, the SLIC lines having certain probabilities, i.e. costs assigned to each line are transferred to a point layer containing nodes wherever two or more SLIC lines intersect. (ii) Second, these nodes are used for a semi-automatic delineation of final boundaries through a human operator (Figure 17a). Both parts are implemented in a publicly available QGIS plugin [95] with a Graphical User Interface (GUI) shown in Figure 17b.

In (i), the SLIC line segments are transferred to a network with nodes on each intersection of two or more SLIC lines and the nodes are displayed to the user. In (ii), the user is asked to select two or more nodes along a land parcel boundary. These are then automatically connected based on the Steiner tree method [98]. This method searches the least-cost path along the remaining SLIC outlines between the nodes that the user selects. A sinuosity measure is calculated for the created line, in order to provide the user with an indication on the line's usability. Sinuosity measures to which extent a line between two points varies from their direct connection, i.e., the ratio between the Euclidean distance between two points and the length of the line connecting the two points. The range of the sinuosity measure is [0; 1]. It is equally divided into three parts to color the line according to a traffic light evaluation system in red, yellow and green. The line is displayed accordingly to indicate the line's usability to the user. Thereafter, the user has the option to simplify the created line, which is done based on the Douglas-Peucker approach [99]. This algorithm simplifies the line by creating a curve along a series of points and gradually reducing the number of points. The user further has the option to manually edit the line or specific nodes of the line by making use of the extensive QGIS editing functionalities [100]. Further options consist of deleting or accepting the line. Choosing the latter, leads to a display of the initial nodes and the request to select a new set of nodes to be connected.

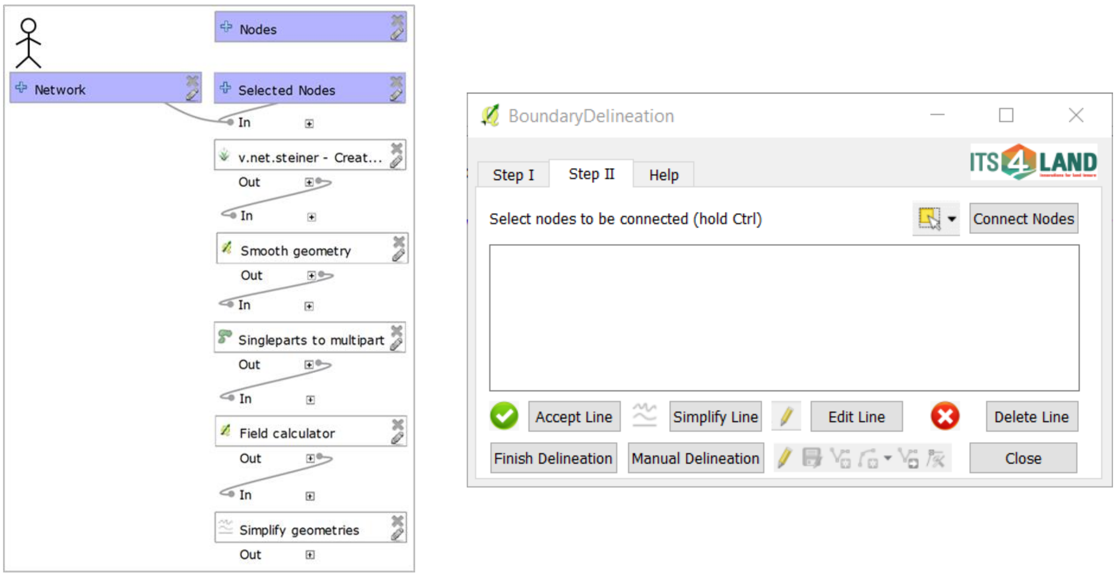

(a) (b)

Figure 17. (**a**) QGIS processing model of the BoundaryDelineation QGIS plugin [95] and (**b**) its graphical user interface (GUI).

4.1.2. Realization

The QGIS plugin (Figure 18) is implemented in Python making use of open source GIS processing modules from GRASS [79], QGIS [101] and GDAL [102]. The plugin can be downloaded via the QGIS plugin repository by searching for 'BoundaryDelineation' (Figure 19). The source code, as well as test data are publically available via GitHub [103]. This repository furthermore provides a manual describing how to install and use the plugin. Its use is further demonstrated in a YouTube video (Figure 20). Links to resources are gathered on the its4land project website as well.

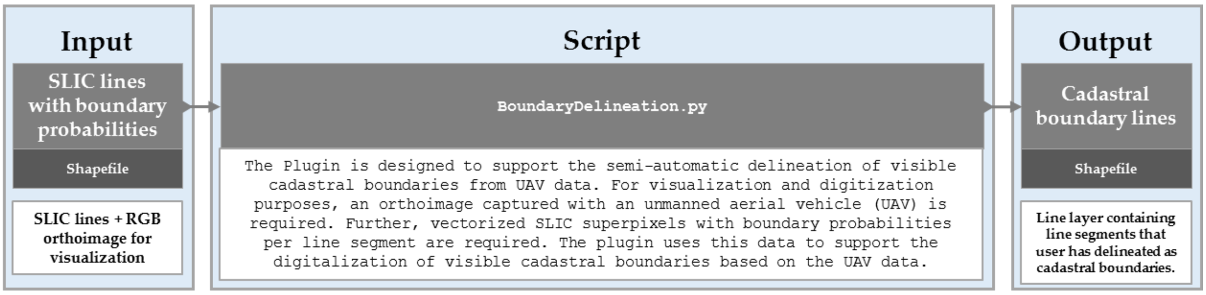

Figure 18. Schematic representation BoundaryDelineation QGIS plugin script available in [103].

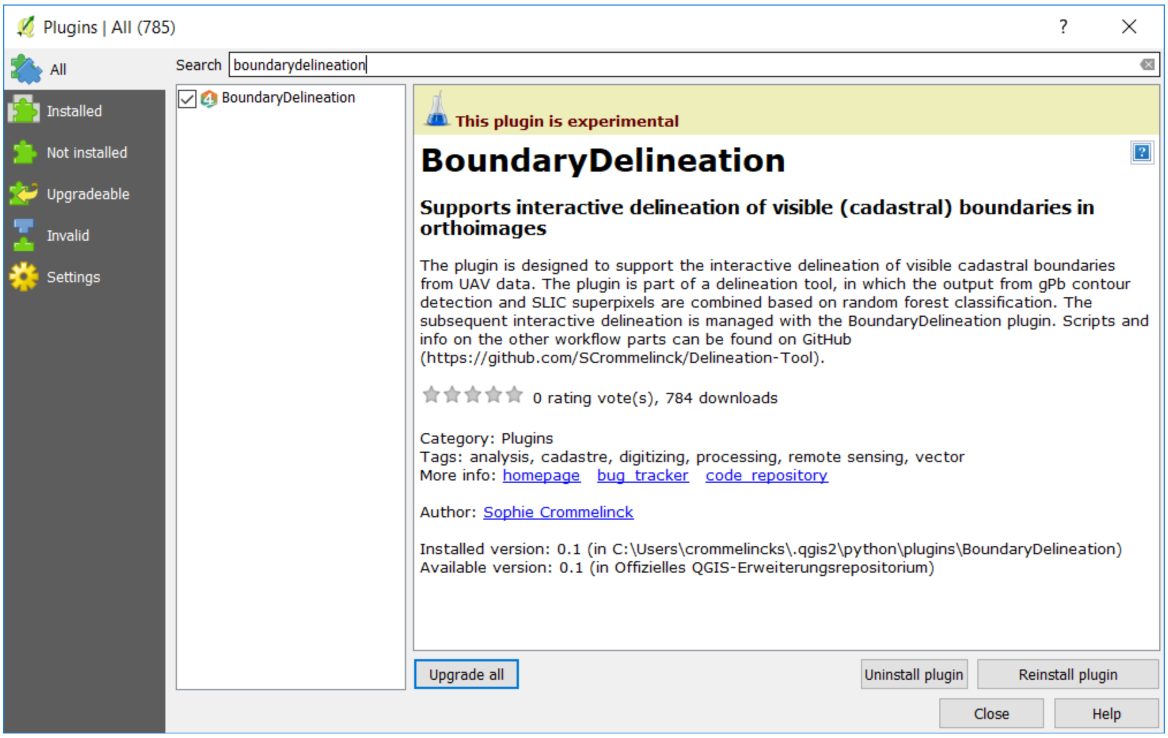

Figure 19. BoundaryDelineation plugin publically available in official QGIS plugin repository [95].

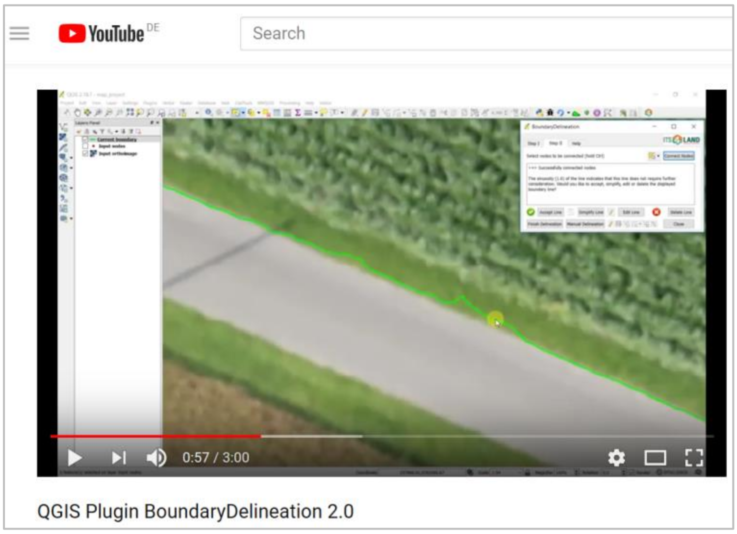

Figure 20. Screenshot of YouTube video demonstrating the use of the BoundaryDelineation plugin.

5. Conclusion

The work presented in this report contributes to advancements in developing a methodology for UAV-based delineation of visible cadastral boundaries. The goal was to develop a methodology for cadastral boundary delineation that is highly automatic, generic and adaptive to different scenarios. This has been addressed by proposing a methodology that partially automates and simplifies the delineation of outlines of physical objects demarcating cadastral boundaries. It is designed for areas, in which physical object contours are clearly visible and coincide with cadastral boundaries. The approach has shown promising results for reducing the effort of current indirect surveying approach based on manual delineation.

In general, the methodology could improve current indirect mapping procedures by making them more reproducible and efficient. However, a certain skill level of the surveyors in geodata processing is required as well as the presence of visible cadastral boundaries. With cadastral boundaries being a human construct, certain boundaries might not be automatically detectable, wherefore semi-automatic approaches are required [104].

Future work could focus on determining optimal features for training [89,105]. The optimal selection of training data could be supported by active learning strategies. Another focus would be extending the approach to different physical objects, datasets and scenarios by developing a classifier transferable across scenes. However, even manually labelling 30% of the data before being able to apply the interactive delineation, would still be superior in terms of effort than delineating 100% manually. Existing cadastral data could be used to automatically generate training data. Further, the least-cost paths generation can be improved by scaling the line costs with their length to avoid the path favoring less segments over lower costs. In addition, sharp edges in the generated least-cost path can be penalized to reduce outlier occurrence, as done in snake approaches.

Besides methodological aspects, future work should focus on the methodology's transferability to real world cadastral mapping scenarios. This will be done in countries like Kenya, Rwanda and Ethiopia, where concepts like fit-for-purpose [21] and responsible land administration [106] are accepted or in place.

With regard to the next deliverable in the its4land project, future work will also concentrate on the integration of existing maps as a source of geometric and semantic information that was left undetected by the automatic feature extraction. Smart sketchmaps that transfer hand-drawn maps into topologically and spatially corrected maps could be integrated in the workflow [107]. This will allow the integration of local spatial knowledge and to delineate socially perceived boundaries, which are not visible to optical sensors.

Future development outside of the its4land project on UAV-based cadastral mapping can be expected, since the ISPRS lists UAVs as key topic and stresses their potential for national mapping in their recent paper on trends and topics for future work [108]. Moreover, the European Union has acknowledge the use of UAV-derived orthoimages as a valid source for as an additional source of information for land policy monitoring [42].

Bibliography

1. Colomina, I.; Molina, P. Unmanned aerial systems for photogrammetry and remote sensing: a review. *ISPRS Journal of Photogrammetry and Remote Sensing* **2014**, *92*, 79-97.

2. Harwin, S.; Lucieer, A. Assessing the accuracy of georeferenced point clouds produced via multi-view stereopsis from unmanned aerial vehicle (UAV) imagery. *Remote Sensing* **2012**, *4*, 1573-1599.

3. Gerke, M.; Przybilla, H.-J. Accuracy analysis of photogrammetric UAV image blocks: Influence of onboard RTK-GNSS and cross flight patterns. *Photogrammetrie-Fernerkundung-Geoinformation* **2016**, *14*, 17-30.

4. Nex, F.; Remondino, F. UAV for 3D mapping applications: a review. *Applied Geomatics* **2014**, *6*, 1-15.

5. Tahar, K.N.; Ahmad, A. An evaluation on fixed wing and multi-rotor UAV images using photogrammetric image processing. *International Journal of Computer, Electrical, Automation, Control and Information Engineering* **2013**, *7*, 48-52.

6. Toth, C.; Jóźków, G. Remote sensing platforms and sensors: A survey. *ISPRS Journal of Photogrammetry and Remote Sensing* **2016**, *115*, 22-36.

7. Rijsdijk, M.; Hinsbergh, W.H.M.V.; Witteveen, W.; Buuren, G.H.M.; Schakelaar, G.a.; Poppinga, G.; Persie, M.V.; Ladiges, R. In *Unmanned aerial systems in the process of juridical verification of cadastral border*, ISPRS - International Archives of the

Photogrammetry, Remote Sensing and Spatial Information Sciences, Rostock, Germany, 2013; *XL-1/W2*, pp 325-331.

8. Eisenbeiss, H.; Sauerbier, M. Investigation of UAV systems and flight modes for photogrammetric applications. *The Photogrammetric Record* **2011**, *26*, 400-421.

9. Fernández-Hernandez, J.; González-Aguilera, D.; Rodríguez-Gonzálvez, P.; Mancera-Taboada, J. Image-based modelling from Unmanned Aerial Vehicle (UAV) photogrammetry: An effective, low-cost tool for archaeological applications. *Archaeometry* **2015**, *57*, 128-145.

10. Zhang, C.; Kovacs, J.M. The application of small unmanned aerial systems for precision agriculture: a review. *Precision Agriculture* **2012**, *13*, 693-712.

11. Berni, J.; Zarco-Tejada, P.; Suárez, L.; González-Dugo, V.; Fereres, E. In *Remote sensing of vegetation from UAV platforms using lightweight multispectral and thermal imaging sensors*, ISPRS - International Archives of the Photogrammetry, Remote Sensing and Spatial Information Sciences, 2009; *XXXVIII-8*, pp 1-6.

12. Puri, A.; Valavanis, K.; Kontitsis, M. In *Statistical profile generation for traffic monitoring using real-time UAV based video data*, Mediterranean Conference on Control & Automation, Athens, Greece, 2007; pp 1-6.

13. Bendea, H.; Boccardo, P.; Dequal, S.; Giulio Tonolo, F.; Marenchino, D.; Piras, M. In *Low cost UAV for post-disaster assessment*, ISPRS - International Archives of the Photogrammetry, Remote Sensing and Spatial Information Sciences, Beijing, China, 2008; *XXXVII-B8*, pp 1373-1379.

14. Chou, T.-Y.; Yeh, M.-L.; Chen, Y.C.; Chen, Y.H. In *Disaster monitoring and management by the unmanned aerial vehicle technology*, Proceedings of the ISPRS TC VII Symposium, Vienna, Austria, 2010; *XXXVVII-7B*, pp 137-142.

15. Irschara, A.; Kaufmann, V.; Klopschitz, M.; Bischof, H.; Leberl, F. In *Towards fully automatic photogrammetric reconstruction using digital images taken from UAVs*, Proceedings of the ISPRS TC VII Symposium, Vienna, Austria, 2010.

16. Binns, B.O.; Dale, P.F. Cadastral surveys and records of rights in land administration. Available online: http://www.fao.org/docrep/006/v4860e/v4860e03.htm (accessed on 10 November 2016).

17. Williamson, I.; Enemark, S.; Wallace, J.; Rajabifard, A. *Land administration for sustainable development*. ESRI Press Academic: Redlands, CA, USA, 2010; p 472.

18. Alemie, B.K.; Bennett, R.M.; Zevenbergen, J. Evolving urban cadastres in Ethiopia: The impacts on urban land governance. *Land Use Policy* **2015**, *42*, 695-705.

19. Nations, U. *Land administrtation in the UNECE Region: Development trends and main principles*. UNECE Information Service: Geneva, 2005; p 103.

20. Kelm, K. UAVs revolutionise land administration. *GIM International* **2014**, *28*, 35-37.

21. Enemark, S.; Bell, K.C.; Lemmen, C.; McLaren, R. *Fit-for-purpose land administration*. Int. Federation of Surveyors: Frederiksberg, Denmark, 2014; p 42.

22. Zevenbergen, J.; Augustinus, C.; Antonio, D.; Bennett, R. Pro-poor land administration: Principles for recording the land rights of the underrepresented. *Land Use Policy* **2013**, *31*, 595-604.

23. Zevenbergen, J.; De Vries, W.; Bennett, R.M. *Advances in Responsible Land Administration*. CRC Press: Padstow, UK, 2015; p 279.

24. Maurice, M.J.; Koeva, M.N.; Gerke, M.; Nex, F.; Gevaert, C. In *A photogrammetric approach for map updating using UAV in Rwanda*, GeoTechRwanda, Kigali, Rwanda, 2015; pp 1-8.

25. Mumbone, M.; Bennett, R.; Gerke, M.; Volkmann, W. In *Innovations in boundary mapping: Namibia, customary lands and UAVs*, World Bank Conference on Land and Poverty, Washington DC, USA, 2015; pp 1-22.

26. Volkmann, W.; Barnes, G. In *Virtual surveying: Mapping and modeling cadastral boundaries using Unmanned Aerial Systems (UAS)*, FIG Congress: Engaging the Challenges - Enhancing the Relevance, Kuala Lumpur, Malaysia, 2014; pp 1-13.

27. Barthel, K. Linking land policy, geospatial technology and community participation. Available online: http://thelandalliance.org/2015/06/early-lessons-learned-from-testing-uavs-for-geospatial-data-collection-and-participatory-mapping/ (accessed on 10 June 2016).

28. Pajares, G. Overview and current status of remote sensing applications based on unmanned aerial vehicles (UAVs). *Photogrammetric Engineering & Remote Sensing* **2015**, *81*, 281-329.

29. Everaerts, J. In *The use of unmanned aerial vehicles (UAVs) for remote sensing and mapping*, ISPRS - International Archives of the Photogrammetry, Remote Sensing and Spatial Information Sciences, 2008; *XXXVII-B1*, pp 1187-1192.

30. Remondino, F.; Barazzetti, L.; Nex, F.; Scaioni, M.; Sarazzi, D. In *UAV photogrammetry for mapping and 3D modeling–current status and future perspectives*, ISPRS - International Archives of the Photogrammetry, Remote Sensing and Spatial Information Sciences, Zurich, Switzerland, 2011; *XXXVIII-1/C22*, pp 25-31.

31. Watts, A.C.; Ambrosia, V.G.; Hinkley, E.A. Unmanned aircraft systems in remote sensing and scientific research: Classification and considerations of use. *Remote Sensing* **2012**, *4*, 1671-1692.

32. Ali, Z.; Tuladhar, A.; Zevenbergen, J. An integrated approach for updating cadastral maps in Pakistan using satellite remote sensing data. *International Journal of Applied Earth Observation and Geoinformation* **2012**, *18*, 386-398.

33. Corlazzoli, M.; Fernandez, O. In *SPOT 5 cadastral validation project in Izabal, Guatemala,* ISPRS - International Archives of the Photogrammetry, Remote Sensing and Spatial Information Sciences, 2004; *XXXV-7/W4,* pp 291-296.

34. Konecny, G. Cadastral mapping with earth observation technology. In *Geospatial Technology for Earth Observation*, Li, D.; Shan, J.; Gong, J., Eds. Springer: 2010; pp 397-409.

35. Ondulo, J.-D. In *High spatial resolution satellite imagery for Pid improvement in Kenya,* FIG Congress: Shaping the Change, Munich, Germany, 2006; pp 1-9.

36. Tuladhar, A. In *Spatial Cadastral Boundary Concepts and Uncertainty in Parcel-Based Information Systems,* ISPRS - International Archives of the Photogrammetry, Remote Sensing and Spatial Information Sciences, 1996; *XXXI-3,* pp 890-893.

37. Christodoulou, K.; Tsakiri-Strati, M. In *Combination of satellite image Pan IKONOS-2 with GPS in cadastral applications,* Workshop on Spatial Information Management for Sustainable Real Estate Market, Athens, Greece, 2002; pp 1-4.

38. Alkan, M.; Marangoz, M. Creating cadastral maps in rural and urban areas of using high resolution satellite imagery. *Applied Geo-informatics for Society and Environment* **2009**, 89-95.

39. Törhönen, M.P. Developing land administration in Cambodia. *Computers, Environment and Urban Systems* **2001**, *25*, 407-428.

40. Greenwood, F. Mapping in practise. In *Drones and Aerial Observation*, New America: 2015; pp 49-55.

41. Manyoky, M.; Theiler, P.; Steudler, D.; Eisenbeiss, H. In *Unmanned aerial vehicle in cadastral applications,* ISPRS - International Archives of the Photogrammetry, Remote Sensing and Spatial Information Sciences, Zurich, Switzerland, 2011; *XXXVIII-1/C22,* p 57.

42. Mesas-Carrascosa, F.J.; Notario-García, M.D.; de Larriva, J.E.M.; de la Orden, M.S.; Porras, A.G.-F. Validation of measurements of land plot area using UAV imagery. *International Journal of Applied Earth Observation and Geoinformation* **2014**, *33*, 270-279.

43. van Hinsberg, W.; Rijsdijk, M.; Witteveen, W. UAS for cadastral applications: testing suitability for boundary identification in urban areas. *GIM International* **2013**, *27*, 17-21.

44. Cunningham, K.; Walker, G.; Stahlke, E.; Wilson, R. In *Cadastral audit and assessments using unmanned aerial systems*, Proceedings of ISPRS and UAV-g, Zurich, Switzerland, 2011; pp 1-4.

45. Cramer, M.; Bovet, S.; Gültlinger, M.; Honkavaara, E.; McGill, A.; Rijsdijk, M.; Tabor, M.; Tournadre, V. In *On the use of RPAS in national mapping—the EuroSDR point of view*, ISPRS - International Archives of the Photogrammetry, Remote Sensing and Spatial Information Sciences, Rostock, Germany, 2013; Copernicus Publications: *XL-1/W2*, pp 93-99.

46. Haarbrink, R. In *UAS for geo-information: Current status and perspectives*, ISPRS - International Archives of the Photogrammetry, Remote Sensing and Spatial Information Sciences, Zurich, Switzerland, 2011; *XXXVIII-1/C22*, pp 1-6.

47. Eyndt, T.; Volkmann, W. UAS as a tool for surveyors: from tripods and trucks to virtual surveying. *GIM International* **2013**, *27*, 20-25.

48. Barnes, G.; Volkmann, W. High-resolution mapping with unmanned aerial systems. *Surveying and Land Information Science* **2015**, *74*, 5-13.

49. Jazayeri, I.; Rajabifard, A.; Kalantari, M. A geometric and semantic evaluation of 3D data sourcing methods for land and property information. *Land Use Policy* **2014**, *36*, 219-230.

50. Zevenbergen, J.; Bennett, R. In *The visible boundary: more than just a line between coordinates*, GeoTechRwanda, Kigali, Rwanda, 18-20 November, 2015; pp 1-4.

51. Bennett, R.; Kitchingman, A.; Leach, J. On the nature and utility of natural boundaries for land and marine administration. *Land Use Policy* **2010**, *27*, 772-779.

52. Dale, P.; McLaughlin, J. *Land administration*. University Press: Oxford, 1999; p 182.

53. Ondulo, J.D.; Wayumba, G.; Aduol, F.W.O. Accuracy Assessment Of Preliminary Index Diagrams (PIDS) From High Resolution Orthoimages In Kenya. *International Journal of Scientific Research and Engineering Studies* **2015**, *2*, 38-44.

54. Cay, T.; Corumluoglu, O.; Iscan, F. In *A study on productivity of satellite images in the planning phase of land consolidation projects*, ISPRS Congress: Geo-Imagery Bridging Continents, Istanbul, Turkey, 2004; pp 1-6.

55. Barnes, G.; Moyer, D.D.; Gjata, G. Evaluating the effectiveness of alternative approaches to the surveying and mapping of cadastral parcels in Albania. *Computers, Environment and Urban Systems* **1994**, *18*, 123-131.

56. Lemmen, C.; Zevenbergen, J.A.; Lengoiboni, M.; Deininger, K.; Burns, T. In *First experiences with high resolution imagery based adjudication approach for social tenure domain model in Ethiopia*, Proceedings FIG-World Bank Conference, Washington DC, USA, March, 2009; pp 9-10.

57. Rao, S.; Sharma, J.; Rajashekar, S.; Rao, D.; Arepalli, A.; Arora, V.; Singh, R.; Kanaparthi, M. In *Assessing usefulness of High-Resolution Satellite Imagery (HRSI) for re-survey of cadastral maps*, ISPRS Annals of the Photogrammetry, Remote Sensing and Spatial Information Sciences, Hyderabad, India, 2014; *II-8*, pp 133-143.

58. Quackenbush, L.J. A review of techniques for extracting linear features from imagery. *Photogrammetric Engineering & Remote Sensing* **2004**, *70*, 1383-1392.

59. Fortin, M.-J.; Olson, R.; Ferson, S.; Iverson, L.; Hunsaker, C.; Edwards, G.; Levine, D.; Butera, K.; Klemas, V. Issues related to the detection of boundaries. *Landscape Ecology* **2000**, *15*, 453-466.

60. Edwards, G.; Lowell, K.E. Modeling uncertainty in photointerpreted boundaries. *Photogrammetric Engineering & Remote Sensing* **1996**, *62*, 377-390.

61. Aien, A.; Kalantari, M.; Rajabifard, A.; Williamson, I.; Bennett, R. In *Advanced principles of 3D cadastral data modelling*, 2nd International Workshop on 3D Cadastres, Delft, the Netherlands, 2011; pp 377-396.

62. Ali, Z.; Ahmed, S. In *Extracting parcel boundaries from satellite imagery for a Land Information System*, International Conference on Recent Advances in Space Technologies (RAST), Istanbul, Turkey, 2013; pp 79-81.

63. Crommelinck, S.; Bennett, R.; Gerke, M.; Nex, F.; Yang, M.Y.; Vosselman, G. Review of automatic feature extraction from high-resolution optical sensor data for UAV-based cadastral mapping. *Remote Sensing* **2016**, *8*, 1-28.

64. Crommelinck, S.; Bennett, R.; Gerke, M.; Yang, M.Y.; Vosselman, G. Contour detection for UAV-based cadastral mapping. *Remote Sensing* **2017**, *9*, 1-13.

65. Crommelinck, S.; Bennett, R.; Gerke, M.; Koeva, M.; Yang, M.Y.; Vosselman, G. SLIC superpixels for object delineation from UAV data. *ISPRS Annals of the Photogrammetry, Remote Sensing and Spatial Information Sciences* **2017**, *IV-2/W3*, 9-16.

66. Crommelinck, S. Delineation-Tool GitHub. Available online: https://github.com/SCrommelinck/Delineation-Tool (accessed on 14 Dec. 2017).

67. Arbelaez, P.; Maire, M.; Fowlkes, C.; Malik, J. Contour detection and hierarchical image segmentation. *Pattern Analysis and Machine Intelligence* **2011**, *33*, 898-916.

68. Arbeláez, P.; Fowlkes, C.; Martin, D. Berkeley segmentation dataset and benchmark. Available online: https://www2.eecs.berkeley.edu/Research/Projects/CS/vision/bsds/ (accessed on 10 Nov. 2016).

69. MathWorks. Available online: www.mathworks.com (accessed on 10 June 2016).

70. Arbeláez, P.; Maire, M.; Fowlkes, C.; Malik, J. Contour detection and image segmentation resources. Available online: https://www2.eecs.berkeley.edu/Research/Projects/CS/vision/grouping/resources.html (accessed on 10 November 2016).

71. Ren, X.; Malik, J. In *Learning a classification model for segmentation*, Int. Conf. on Computer Vision (ICCV), Washington, DC, US, 13-16 October, 2003; IEEE: *1*, pp 10-17.

72. Neubert, P.; Protzel, P. In *Superpixel benchmark and comparison*, Proc. Forum Bildverarbeitung, Regensburg, Germany, 29-30 November, 2012; pp 1-12.

73. Csillik, O. In *Superpixels: the end of pixels in OBIA. A comparison of stat-of-the-art superpixel methods for remote sensing data*, GEOBIA, Enschede, the Netherlands, 14-16 September, 2016; pp 1-5.

74. Schick, A.; Fischer, M.; Stiefelhagen, R. In *Measuring and evaluating the compactness of superpixels*, Int. Conf. on Pattern Recognition (ICPR), Tsukuba Science City, Japan, 11-15 November, 2012; pp 930-934.

75. Stutz, D.; Hermans, A.; Leibe, B. Superpixels: an evaluation of the state-of-the-art. *Computer Vision and Image Understanding* **2017**, 1-32.

76. Achanta, R.; Shaji, A.; Smith, K.; Lucchi, A.; Fua, P.; Süsstrunk, S. *SLIC superpixels*; 2010.

77. Achanta, R.; Shaji, A.; Smith, K.; Lucchi, A.; Fua, P.; Susstrunk, S. SLIC superpixels compared to state-of-the-art superpixel methods. *IEEE Transactions on Pattern Analysis and Machine Intelligence* **2012**, *34*, 2274-2282.

78. Kanavath, R.; Metz, M. GRASS SLIC superpixels. Available online: https://grass.osgeo.org/grass72/manuals/addons/i.superpixels.slic.html (accessed on 4 Dec. 2017).

79. GRASS Development Team. Geographic Resources Analysis Support System (GRASS) Software, version 7.0. Available online: https://grass.osgeo.org/ (accessed on 3 March 2017).

80. Levinshtein, A.; Sminchisescu, C.; Dickinson, S. Optimal image and video closure by superpixel grouping. *Int. Journal of Computer Vision* **2012**, *100*, 99-119.

81. Levinshtein, A.; Sminchisescu, C.; Dickinson, S. In *Optimal contour closure by superpixel grouping*, European Conf. on Computer Vision, Crete, Greece, 5-11 September, 2010; Daniilidis, K.; Maragos, P.; Paragios, N., Eds. Springer: pp 480-493.

82. Sowmya, A.; Trinder, J. Modelling and representation issues in automated feature extraction from aerial and satellite images. *ISPRS Journal of Photogrammetry and Remote Sensing* **2000**, *55*, 34-47.

83. Iqbal, Q.; Aggarwal, J.K. Retrieval by classification of images containing large manmade objects using perceptual grouping. *Pattern Recognition* **2002**, *35*, 1463-1479.

84. Stahl, J.S.; Wang, S. Edge grouping combining boundary and region information. *IEEE Transactions on Image Processing* **2007**, *16*, 2590-2606.

85. Estrada, F.J.; Jepson, A.D. In *Perceptual grouping for contour extraction*, Proc. 17th Int. Conf. on Pattern Recognition (ICPR), 2004; *2*, pp 32-35.

86. Turker, M.; Kok, E.H. Field-based sub-boundary extraction from remote sensing imagery using perceptual grouping. *ISPRS Journal of Photogrammetry and Remote Sensing* **2013**, *79*, 106-121.

87. Yang, J.; Wang, R. Classified road detection from satellite images based on perceptual organization. *Int. Journal of Remote Sensing* **2007**, *28*, 4653-4669.

88. Lowe, D. *Perceptual organization and visual recognition*. Springer: 1985; Vol. 5, p 162.

89. Warnke, S.; Bulatov, D. In *Variable selection for road segmentation in aerial images*, Int. Archives of the Photogrammetry, Remote Sensing and Spatial Information Sciences, Hannover, Germany, 6–9 June, 2017; *XLII-1/W1*, pp 297-304.

90. García-Pedrero, A.; Gonzalo-Martín, C.; Lillo-Saavedra, M. A machine learning approach for agricultural parcel delineation through agglomerative segmentation. *Int. Journal of Remote Sensing* **2017**, *38*, 1809-1819.

91. Yang, M.Y.; Rosenhahn, B. Superpixel cut for figure-ground image segmentation. *ISPRS Annals of the Photogrammetry, Remote Sensing and Spatial Information Sciences* **2016**, *III-3*, 387-394.

92. Santana, T.M.H.C.; Machado, A.M.C.; de A. Araújo, A.; dos Santos, J.A. In *Star: a contextual description of superpixels for remote sensing image classification*, Progress in Pattern Recognition, Image Analysis, Computer Vision, and Applications, Lima, Peru, 8–11 November, 2017; Beltrán-Castañón, C.; Nyström, I.; Famili, F., Eds. Springer Int. Publishing: pp 300-308.

93. Wang, X.-Y.; Wu, C.-W.; Xiang, K.; Chen, W. Efficient local and global contour detection based on superpixels. *Journal of Visual Communication and Image Representation* **2017**, *48*, 77-87.

94. Jiang, H.; Wu, Y.; Yuan, Z. In *Probabilistic salient object contour detection based on superpixels*, Conf. on Image Processing (ICIP), Melbourne, Australia, 15-18 September, 2013; pp 3069-3072.

95. Crommelinck, S. QGIS Python Plugins Repository: BoundaryDelineation. Available online: http://plugins.qgis.org/plugins/BoundaryDelineation/ (accessed on 13 June 2017).

96. Pedregosa, F.; Varoquaux, G.; Gramfort, A.; Michel, V.; Thirion, B.; Grisel, O.; Blondel, M.; Prettenhofer, P.; Weiss, R.; Dubourg, V., *et al.* Scikit-learn: Machine Learning in Python. *Journal of Machine Learning Research* **2011**, *12*, 2825-2830.

97. Scikit RandomForestClassifier. Available online: http://scikit-learn.org/stable/modules/generated/sklearn.ensemble.RandomForestClassifier.html (accessed on 27 october 2017).

98. Hwang, F.; Richards, D.S. Steiner tree problems. *Networks* **1992**, *22*, 55-89.

99. Saalfeld, A. Topologically consistent line simplification with the Douglas-Peucker algorithm. *Cartography and Geographic Information Science* **1999**, *26*, 7-18.

100. QGIS Development Team. QGIS Editing. Available online: https://docs.qgis.org/2.2/en/docs/user_manual/working_with_vector/editing_geometry_attributes.html (accessed on 10 May 2017).

101. QGIS Development Team. QGIS geographic information system, open source geospatial foundation. Available online: www.qgis.org (accessed on 3 March 2017).

102. GDAL Development Team. GDAL - Geospatial Data Abstraction Library, Version 2.1.2. Open Source Geospatial Foundation. Available online: www.gdal.org (accessed on 3 March 2017).

103. Crommelinck, S. BoundaryDelineation GitHub. Available online: https://github.com/SCrommelinck/BoundaryDelineation (accessed on 17 May 2017).

104. Luo, X.; Bennett, R.; Koeva, M.; Lemmen, C.; Quadros, N. Quantifying the overlap between cadastral and visual boundaries: a case study from Vanuatu. *Urban Science* **2017**, *1*, 32.

105. Genuer, R.; Poggi, J.-M.; Tuleau-Malot, C. Variable selection using random forests. *Pattern Recognition Letters* **2010**, *31*, 2225-2236.

106. Zevenbergen, J.; De Vries, W.; Bennett, R. *Advances in responsible land administration*. CRC Press: Padstow, UK, 2015; p 279.

107. Schwering, A.; Wang, J.; Chipofya, M.; Jan, S.; Li, R.; Broelemann, K. SketchMapia: Qualitative representations for the alignment of sketch and metric maps. *Spatial Cognition and Computation* **2014**, *14*, 220-254.

108. Chen, J.; Dowman, I.; Li, S.; Li, Z.; Madden, M.; Mills, J.; Paparoditis, N.; Rottensteiner, F.; Sester, M.; Toth, C., *et al.* Information from imagery: ISPRS scientific vision and research agenda. *ISPRS Journal of Photogrammetry and Remote Sensing* **2016**, *115*, 3-21.